Cells and Materials

Volume 5 | Number 1 Article 2

1995

Three-Dimensional Morphology and Platelet Adhesion on Pyrolytic Carbon Heart Valve Materials

S. L. Goodman
University of Wisconsin, Madison

K. S. Tweden
St. Jude Medical, Inc., St. Paul

R. M. Albrecht
University of Wisconsin, Madison

Cells and Materials, Vol. 5, No. 1, 1995 (Pages 15-30) 1051-6794/95$5.00+.25
Scanning Microscopy International, Chicago (AMF O'Hare), IL 60666 USA

THREE-DIMENSIONAL MORPHOLOGY AND PLATELET ADHESION ON PYROLYTIC CARBON HEART VALVE MATERIALS

S.L. Goodman*, K. S. Tweden[1] and R.M. Albrecht

Dept. Animal Health and Biomedical Sciences, University of Wisconsin, 1655 Linden Drive, Madison, WI 53706
[1]St. Jude Medical, Inc., One Lillehei Plaza, St. Paul, MN 55117

(Received for publication December 19, 1994 and in revised form April 16, 1995)

Abstract

Low-temperature isotropic pyrolytic carbon (LTIC) is the preferred material for mechanical heart valve prosthetics due to its durability and good thromboresistance, although thromboembolic complications remain a significant clinical problem. LTIC morphology has been previously studied using scanning (SEM) and transmission electron microscopy (TEM), and scanning tunneling microscopy (STM). However, these microscopies have limitations with imaging rough surfaces. In this study, LTIC valve leaflets from CarboMedics, Inc. and St. Jude Medical, Inc. were prepared and polished exactly as used in clinical prosthetics, and examined at magnifications up to macromolecular resolution using stereo-pair low-voltage SEM (LV-SEM). LV-SEM reveals that LTIC leaflets have a complex topography of 10 nm to 1 μm features, with height differences of 100-500 nm occurring over lateral distances of 10-50 nm. Compared to previous reports using conventional SEM and STM, LV-SEM shows a much rougher surface. In contrast to studies that have reported minimal platelet interaction with LTIC, very extensive adhesion and spreading were observed. That our observations are different from previous reports may be explained by the physics of SEM image formation at low and conventional (higher) accelerating voltages. Due to the low atomic density of LTIC and platelets, obscuration of small features due to specimen coatings, and since platelets closely follow LTIC's three-dimensional contours, the surface sensitivity of conventional SEM is unable to provide sufficient contrast to image either the material topography or thin adherent platelets. These results suggest that the extent of platelet interaction on LTIC vascular prosthetics may have been previously underestimated.

Key Words: Pyrolytic carbon, platelets, low voltage scanning electron microscopy, heart valves, thrombosis.

*Address for correspondence:
S.L. Goodman, address as above.
Phone no.: 608-262-0816 / FAX no.: 608-262-7420

Introduction

It is estimated that between 1969 and 1993 over 1.3 million mechanical heart valve prosthetics with low-temperature isotropic pyrolytic carbon (LTIC) components have been implanted world-wide, representing over 8.3 million patient years (personal communication with Dr. Charles Griffin, CarboMedics Inc., Austin, TX). This material, as used in valve prosthetics, is a composite consisting of a graphite substrate coated with a 300-400 μm thick layer of SiC/LTIC alloy, with the silicon alloy used to improve durability. The blood compatibility and durability of LTIC heart valve prostheses is well documented with over 20 years of success [8]. Nonetheless, a small but significant percentage of valve recipients experience thromboembolic and/or hemorrhagic complications. A recent ten-plus year compendium study based on 10 reports found the average complication rates for patients with St. Jude mechanical valves was 1.33% per year for thromboembolic events, 0.15% for valve thrombosis, and 1.06% per year for anticoagulant related hemorrhage [3]. Other studies have reported similar or somewhat poorer performance with valves from several manufacturers [13, 16]. Such complications are the dominant clinical problem with the use of these devices.

The usefulness of LTIC in cardiovascular and other biomaterial applications were largely established by studies performed one or more decade(s) ago [6, 8, 26, 27, 28, 47]. Due to the interest in LTIC and related carbon forms for a variety of applications, many studies have investigated bulk material structure with transmission electron microscopy (TEM) [31, 32, 41, 49], and transmission polarized light microscopy [8]. In biomedical applications, blood and tissue interactions occur at the device surface, thus studies have also investigated LTIC surface structure using scanning electron microscopy (SEM) [6, 8, 31, 32]. Until recently, SEM instrumentation was capable of only relatively low resolution compared to TEM. To provide higher resolution surface imaging, replicas of LTIC surfaces were examined with TEM [7]. Unfortunately, preparing reliable replicas of rough samples is problematic [48]. LTIC has also been

examined with scanning tunneling microscopy (STM) at very high resolution [14, 35, 36]. However, STM and similar instruments (such as the atomic force microscope or AFM) are limited in their ability to image less than smooth samples due to lateral interactions of the mechanical scanning probe with rough surfaces [33]. Thus, our overall understanding of the surface morphology of these materials is limited by instrumental considerations in especially the size range of biological interactions: the size of cells, cell processes, and proteins. With the advent of high-resolution low-voltage SEM (LV-SEM), biological and material morphology in this size range may now be examined. Through the development of cold filament field emission electron sources, low aberration immersion lenses and high sensitivity through-the-lens secondary detectors [37], in combination with an improved understanding of electron beam-specimen interactions and sample preparation, the capability of the SEM has been dramatically improved [30, 38]. These advances enable the attainment of both high resolution and high surface sensitivity on low density and low atomic number materials such as dried biological samples [25, 30, 38, 39] and polymers [19, 24].

In the present study, LV-SEM is used to image the complex three-dimensional (3-D) morphology of LTIC over a range of magnifications up to macromolecular resolution. In the second part of this study, *in vitro* human platelet adhesion is briefly examined. Although many studies have examined the thromboresistant properties of LTIC, and generally reported good antithrombotic properties [13], there has been little recent work on the subject [1, 11], with the exception of clinical case studies of valve recipients, as described above [3, 8, 13, 16]. Early on, it was determined that LTIC tenaciously adsorbs albumin and other proteins from blood [4]. Since adsorbed albumin is well known to minimize platelet adherence, studies investigating the thromboresistance of LTIC have largely focused on the role of adsorbed albumin in passivating material surfaces [12, 14, 27]. This may explain why few studies have directly examined platelet adherence on these materials [5, 13, 42]. By utilizing LV-SEM in the present study, platelet interaction with these clinically important materials is examined with higher resolution and much greater surface sensitivity than was previously possible on these topologically complex surfaces.

Materials and Methods

Materials

Low-temperature isotropic pyrolytic carbon valve leaflets manufactured by both CarboMedics, Inc. (CMI) and by St. Jude Medical, Inc. (SJM) were examined. The LTIC substrate is prepared as previously described [6, 43]. Briefly, the material is manufactured using a chemical vapor deposition and fluidized bed process. Polishing is accomplished using silicon carbide and alumina media. Cleaning of all substrates was performed using a series of ultrasonic baths in detergents, and finishing with isopropanol, as has been described [44]. Identically prepared samples were used for morphological examination and platelet adhesion. Surface chemical analysis and detailed platelet spreading assays will be reported elsewhere (manuscript submitted). In order to fit the sample chamber of the high-resolution SEM, some valve leaflets were cut prior to cleaning. To provide a positive control material for platelet spreading, Formvar (polyvinyl formal) filmed TEM grids were used [22].

Surface morphology

LTIC morphology was examined with stereo-pair high-resolution LV-SEM, using a modified Hitachi S-900 [38, 40]. Uncoated samples were examined at 1.5 keV and at higher accelerating voltages. To provide an accurate 3-D size standard, 100 $\pm$ 0.09 nm or 50 $\pm$ 0.09 nm (mean $\pm$ standard deviation) polystyrene beads (Polysciences, Warrington, PA: #16662 and #8691) were applied to selected samples. These samples were then lightly ion-beam coated (Ion Tech, Teddington, England) with 1-2 nm of Pt, and imaged at SEM accelerating voltages of 1.5-3.5 keV. Stereo-pairs were obtained at $\pm 5°$ from the horizontal. Relative heights (Z) of selected points were calculated from the measured parallax shift (P) in stereo images using the formula:

$$Z = [P / \{2\sin(\alpha/2)\}] \quad (1)$$

where α is the half angle for the stereo-pair [10]. These height measurements are dependent upon the accuracy of the tilt stage, the measurement of the parallax shift, and the accuracy of the lateral magnification. In the present study, the overall accuracy is of two significant figures.

Additional micrographs were obtained with a conventional SEM equipped with a LaB_6 filament operating at accelerating voltages of 15 and 25 keV (Hitachi S-570), and a tungsten filament equipped instrument (JEOL JSM 35C). Samples for these instruments were cold cathode sputter-coated (SeeVac Auto Conductavac IV, Pittsburgh, PA) with 10 nm AuPd, as measured with a crystal oscillator thickness monitor (Inficon XTM, Syracuse, NY).

Primary electron beam paths in LTIC were simulated using a Monte Carlo calculation program kindly provided by Dr. D.C. Joy (Univ. Tennessee, Knoxville) [29, 30]. For the purpose of these calculations, it was assumed that LTIC was composed of 100% carbon at a density of 2 g/cm^3, since density of LTIC typically varies from 1.7 to 2.2 g/cm^3 [6]. Surface analysis (using X-ray photoelectron spectroscopy) indicates that the LTIC surfaces are composed of 82-88% carbon, 9-13%

oxygen, and small to trace amounts of nitrogen, silicon, chlorine, aluminum, and sodium.

Platelet studies

Human platelets were purified from acid-citrate-dextrose (1:9) anticoagulated whole blood by gel filtration [45] of platelet rich plasma, which was prepared by centrifugation at 120 x g for 15 minutes. HEPES-Tyrodes buffer, containing 1 mg/ml bovine serum albumin (BSA; Sigma #A-7888, St. Louis, MO) was used as the platelet suspension buffer and as the column-washing eluent [20, 21, 22]. All platelet donors enrolled in this research have responded to an Informed Consent, and blood is obtained via a Human Subject Committee approved protocol that is reviewed annually by the University of Wisconsin. Platelet adhesion was evaluated by applying platelet suspensions to LTIC samples and to Formvar filmed grids at 37°C. Surfaces were previously hydrated in the HEPES-Tyrodes platelet buffer minus BSA for at least 2 hours at 37°C. Platelets were applied to surfaces for 10 minutes, after which non-adherent

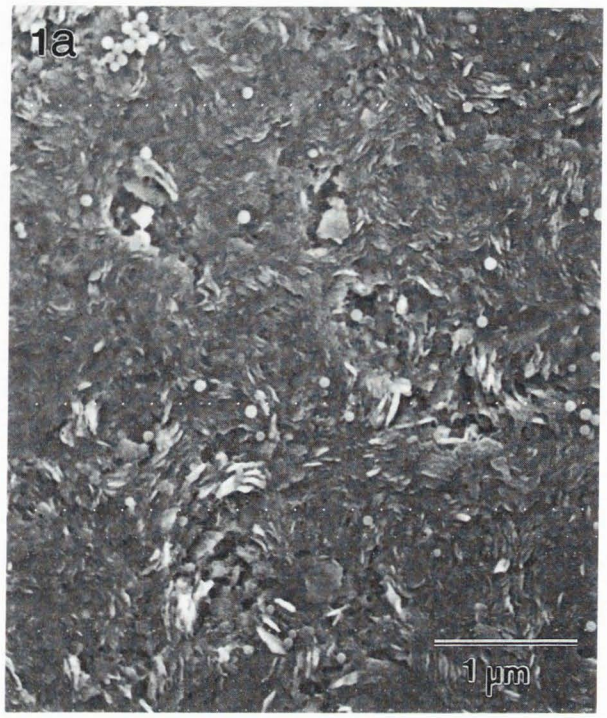

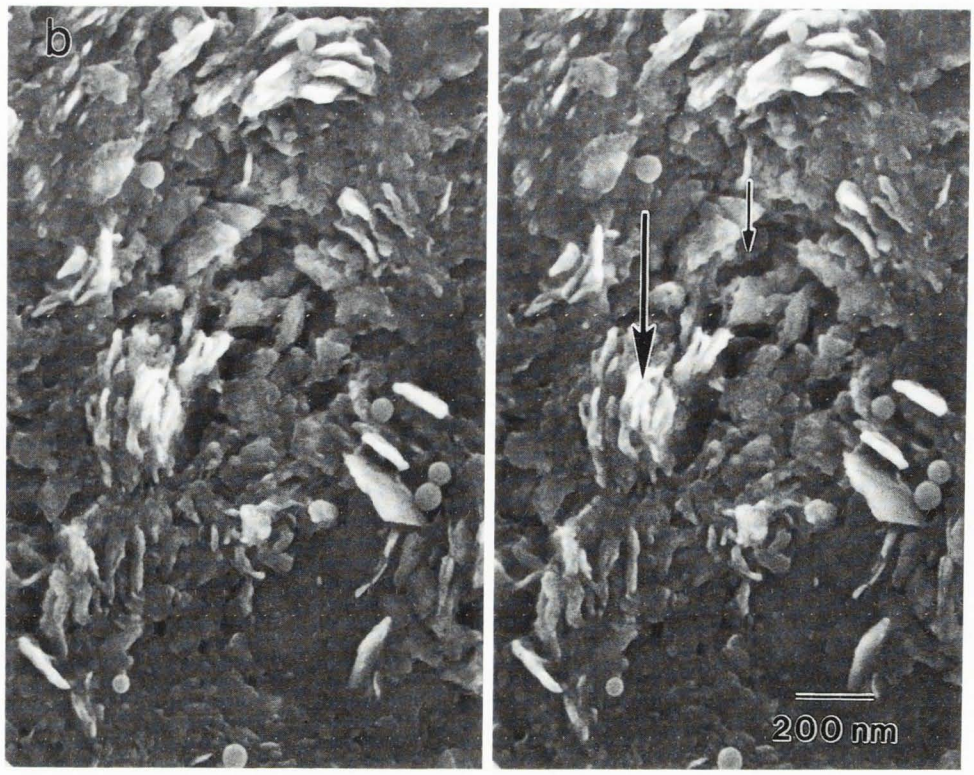

Figure 1. (a) LV-SEM images of SJM-LTIC at 2.5 keV show a very complex surface topography made up of disks of 100-200 nm diameter organized into circular crystallite-like structures of approximately 750-1000 nm, with the "crystallite" circles separated by more amorphous regions. The overall organization appears isotropic. (b) High-resolution stereo-pair of lower left region shows that the disks are 15-30 nm thick and stacked together into clusters of 5-10 elements (large arrow). Stereo imaging shows considerable vertical complexity. The height differences between a depression (small arrow) and the peak of some vertically oriented disks (large arrow) is 300 nm. Ion beam Pt-coated with 100 ± 9 nm spheres added as size standards.

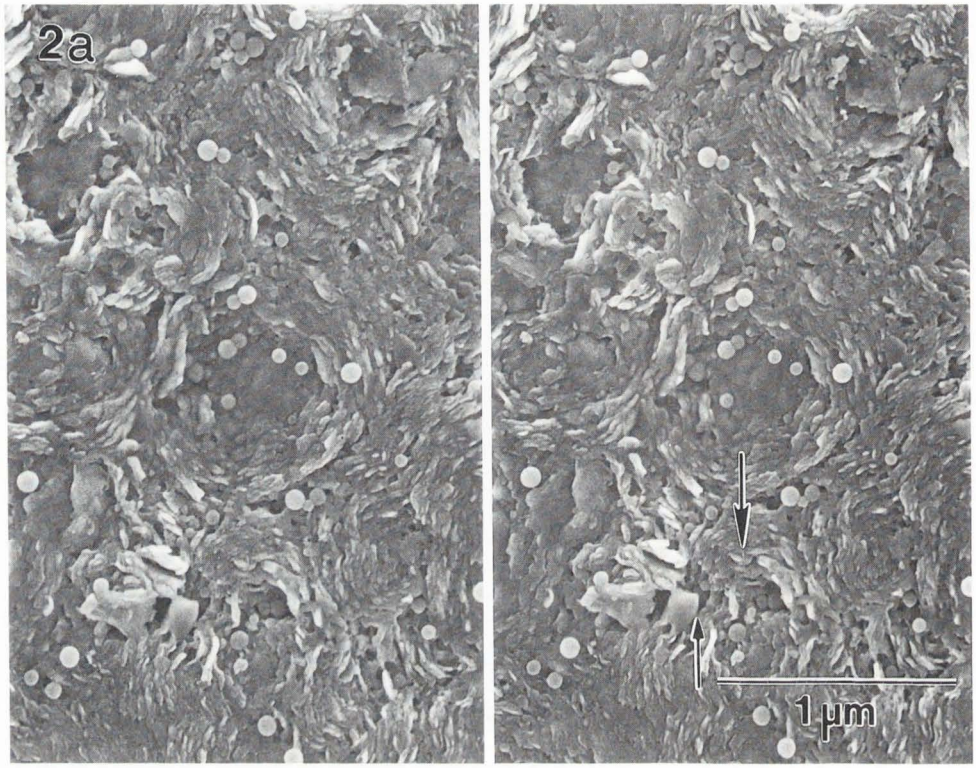

Figure 2. (a) Intermediate magnification stereo-pair LV-SEM image of CMI-LTIC provides an overview of the surface topography and shows the same surface structure as on SJM-LTIC (Fig. 1). A typical depression is indicated, with a height difference of 280 nm from the bottom (small arrow) to a nearby high point (medium arrow). (b) High-resolution image of central region shows the fine extent of LTIC structure. This image is at the limit of resolution obtainable with this lightly Pt-coated sample at 2.5 keV. Edge-on and plane views show that the disks appear to be composed of fused 15-30 nm particles. Minor edge effect brightening is observed with some disks and on the polystyrene size standards. Ion beam Pt-coated with 50 ± 9 nm spheres added as size standards.

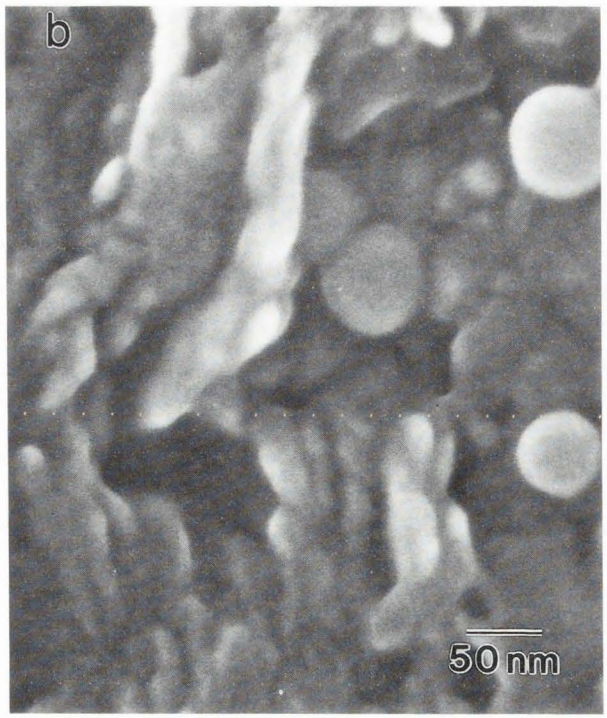

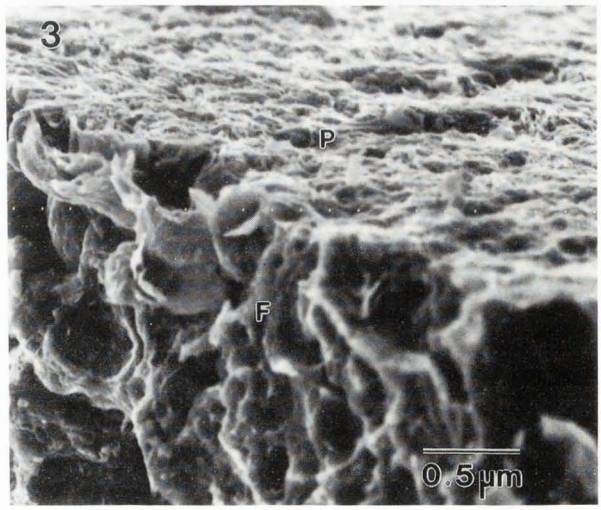

Figure 3. Cross-section of a fractured edge of CMI-LTIC. Note fineness of structure at the polished (P) surface, compared to the more open internal structure exposed at the fractured (F) face. Ion beam Pt-coated, imaged at 2.5 keV.

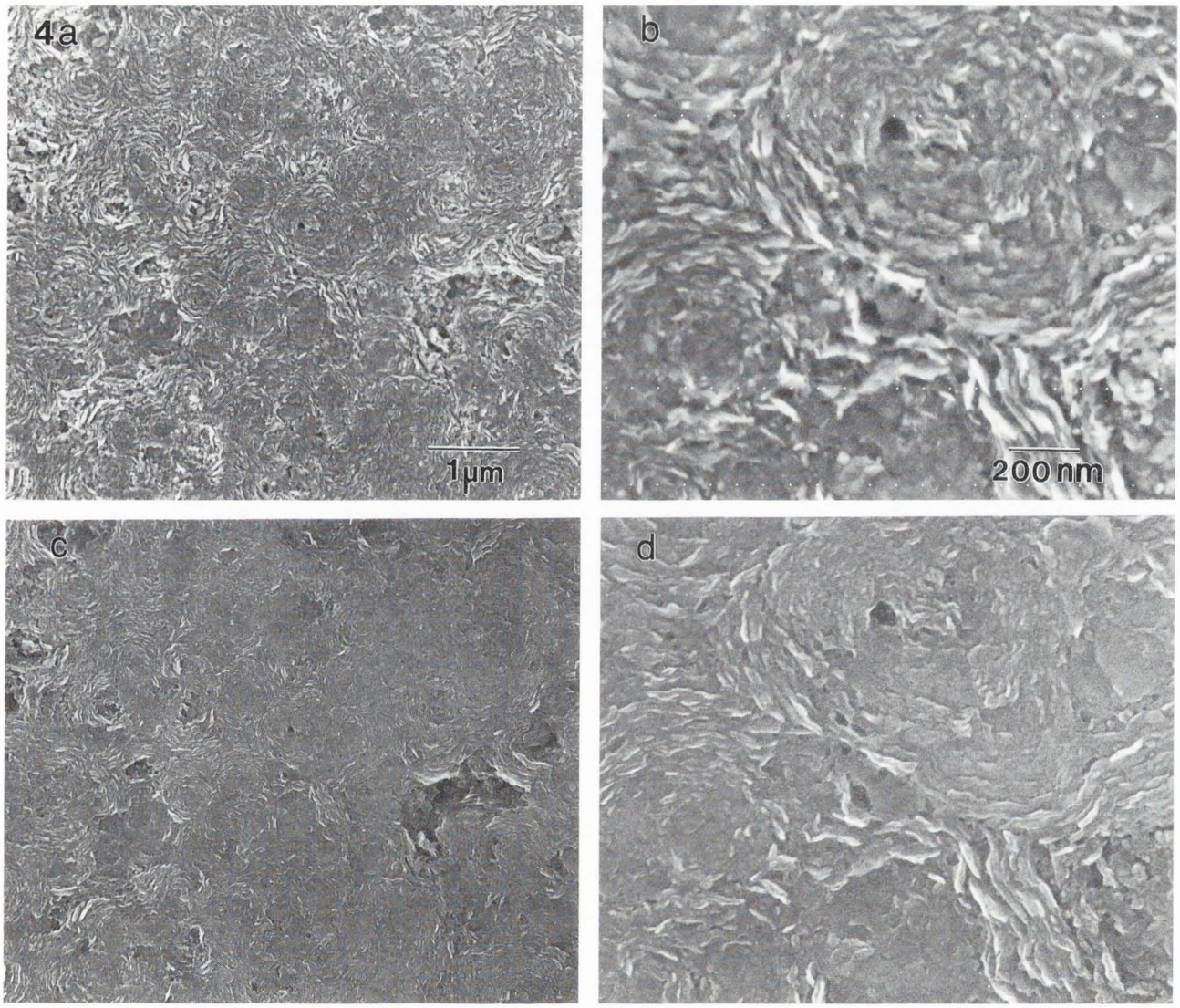

Figure 4. The surface texture of CMI-LTIC appears rougher at 1.5 keV (**a**, **b**) than at 15 keV (**c**, **d**). Figures b and d are of the central regions in a and c. At 15 keV, only the largest features remain visible, while other features become less distinct and more rounded. Sample is uncoated.

platelets were gently rinsed off with suspension buffer and adherent platelets were allowed to continue spreading for an additional 20 minutes.

Adherent platelets were prepared for electron microscopy by fixation in 1% glutaraldehyde for 30 minutes, 15 minutes post-fixation in 0.05% osmium tetroxide in HEPES buffer, serial ethanol dehydration, and drying by the critical point method with carbon dioxide [21, 25, 34]. Samples were then ion-beam coated with 1-2 nm of Pt and imaged at 1.5-2.5 keV. Stereo-pairs were obtained at $\pm 5°$ from the horizontal, and heights calculated as described above. A few samples were also sputter-coated with 10 nm of AuPd for imaging with conventional SEM instrumentation.

Results

Material structure

No differences were apparent between the surface morphologies of the SJM (Fig. 1) and CMI (Fig. 2) materials; both samples have a complex 3-D surface structure with nanometer to micrometer size features. Low magnification images provide an overview of the structure and show depressions of 0.25-0.5 μm width and depth (Figs. 1 and 2). Stereo imaging and parallax measurement permit full appreciation and measurement of the complex surface topography. Overall, Figures 1 and 2 show that the LTIC structure is composed of 15-30 nm thick disks of 100-200 nm diameter, which are

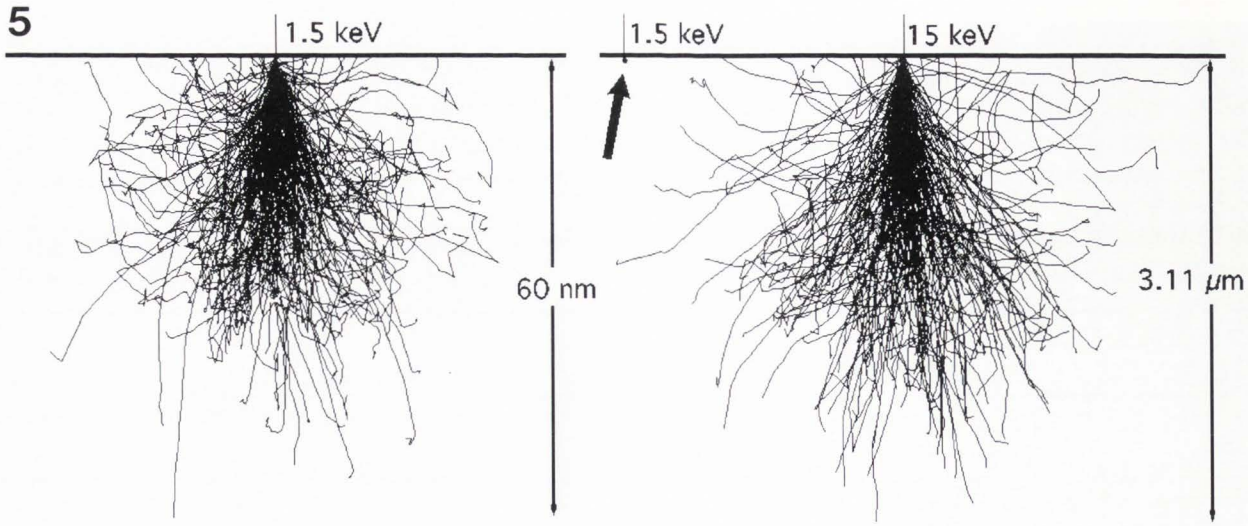

Figure 5. Monte Carlo calculation of electron trajectories in carbon at a density of 2 g/cm^3. At 1.5 keV, the maximum path is 60 nm, while at 15 keV, the maximum path is 3.11 μm. For each simulation, 250 trajectories were calculated. To permit direct comparison between electron-solid interactions at 1.5 and 15 keV, the 1.5 keV trajectories were redrawn to the same scale as used for the 15 keV paths (arrow).

organized into circular crystallite-like structures of approximately 750-1000 nm, with the "crystallite" circles separated by more amorphous regions. The organization of the disks and crystallite circles (composed of disks) appears random. The disks seem to be composed of smooth particles about 15-30 nm in size which are laterally fused to make up their thickness (Fig. 2b). The overall organization gives rise to a complex topography with features in the 10-30 nm range (spacing between disks, disk thickness), 100-200 nm range (disk diameters), and the μm-size range of the crystallite-like circular clusters of disks. Height differences of 100-300 nm are commonly observed over lateral distances as short as 15-30 nm, i.e., the thickness of a single disk.

A fractured sample of CMI-LTIC permits viewing of the cross-sectional morphology of the LTIC layer of a valve leaflet (Fig. 3) and shows that the surface polishing creates a denser and finer structure, as compared to the relative openness of the LTIC below the surface. From such samples, it appears that the polishing and LTIC deposition creates a finer morphology to about 100 nm into the LTIC layer, and that the bulk leaflet structure then remains constant for at least another micron from the surface.

Images of uncoated LTIC obtained at the low accelerating voltage of 1.5 keV (Figs. 4a and 4b) show the same structure as observed in Figures 1 and 2, which were lightly Pt-coated and imaged at 2.5 keV. However, at a conventional SEM accelerating voltage of 15 keV, on this uncoated sample, much finer structure becomes nearly undetectable (Figs. 4c and 4d). At 15 keV, only gross features are readily observed, such as 100 nm pits, while smaller features become considerably less distinct (compare Figs. 4a and 4c). At higher resolution, disks and other fine features appear flat and rounded when imaged at 15 keV (Fig. 4d), as compared to 1.5 keV (Fig. 4b). The overall impression is that the material appears considerably smoother when imaged at 15 keV than at 1.5 keV. Although Figure 4 shows this on uncoated samples, such "smoothing" was also observed on Pt-coated samples including the sample imaged in Figures 1 and 2, and was observed (not shown) at accelerating voltages as low as 3.5 keV at high resolution ($>$ 50,000x).

Monte Carlo simulations of primary beam electron trajectories in carbon at 2 g/cm^3 show that electron paths vary considerably with the accelerating voltage. At 1.5 keV the maximum path length is 60 nm, with most electrons having a considerably shorter path. In contrast, at 15 keV the maximum penetration increases to over 3 μm, with most electrons paths terminating at least 1 μm from the point of entry (Fig. 5). For comparison, at an intermediate accelerating voltage of 5 keV, the calculated maximum path length is 460 nm (not shown).

Platelet adhesion

Platelets applied to Formvar rapidly reached fully-spread morphology, although a few remain in less activated pseudopodial shapes (Fig. 6a). Higher resolution stereo imaging shows considerable Z-axis growth of platelet aggregates, including pseudopods reaching away from the surface 3-5 μm or more (Fig. 6b). The fully-

spread platelets were considerably thinner with thicknesses varying from about 0.25 to 1.5 μm, the thinnest region occurring about 0.25-0.5 μm from the platelet edge (at the outer filamentous zone [22, 34]) and the thickest region generally occurring just peripherally to the central granulomere region (the inner filamentous zone) or over the granulomere region itself (Fig. 6b).

On both CMI-LTIC (Fig. 7) and SJM-LTIC (not shown) almost every platelet directly adherent to the material was fully spread. With few exceptions, all less activated platelets were adherent to (on top of) LTIC surface-adherent fully-spread platelets and virtually the entire surface was covered with spread platelets (Fig. 7a), as compared to a more partial coverage observed on Formvar (Fig. 6a). When the identical sample region in Figure 7a was imaged at 15 keV, fully-spread platelets were more difficult to detect whereas pseudopodial platelets became more obvious due to a greater apparent brightness (Fig. 7b). Higher resolution stereo imaging at 1.5 keV shows that LTIC-adherent platelets were very flat; typically only 0.25-0.5 μm at their thickest point. These fully-spread platelets also very closely followed the contours of the LTIC substrate (Fig. 7c). High resolution showed apparently poor preservation of the membranes of the fully-spread platelets, while the membranes

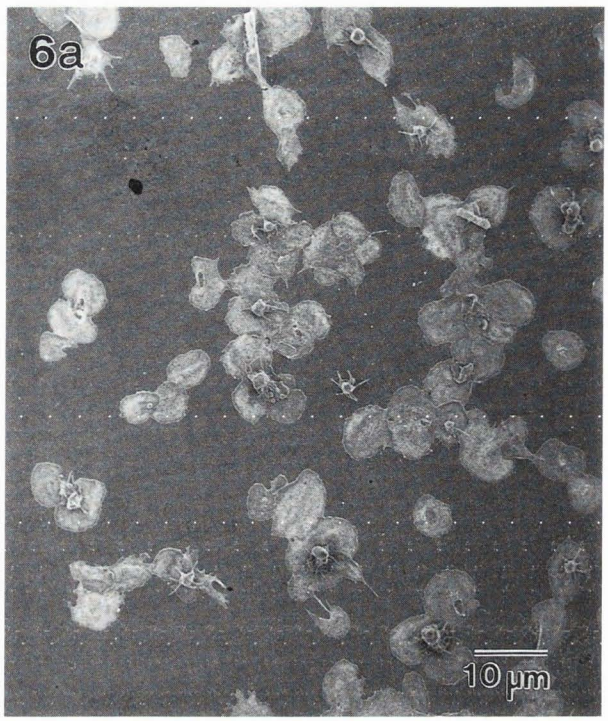

Figure 6. (a) LV-SEM of mostly fully-spread platelets adherent to the Formvar control surface. (b) Stereo-pair of central region shows the heights of the spread and pseudopodial platelets. With the flat Formvar surface as the reference, a point near the edge of a fully-spread platelet is 260 nm high (arrowhead), a point more centrally located on another fully-spread platelet is 1.4 μm high (small arrow), the tip of a pseudopod is 3.2 μm high (medium arrow), and the top of an aggregate is 5.3 μm above the substrate (large arrow). Ion beam Pt-coated, imaged at 1.5 keV.

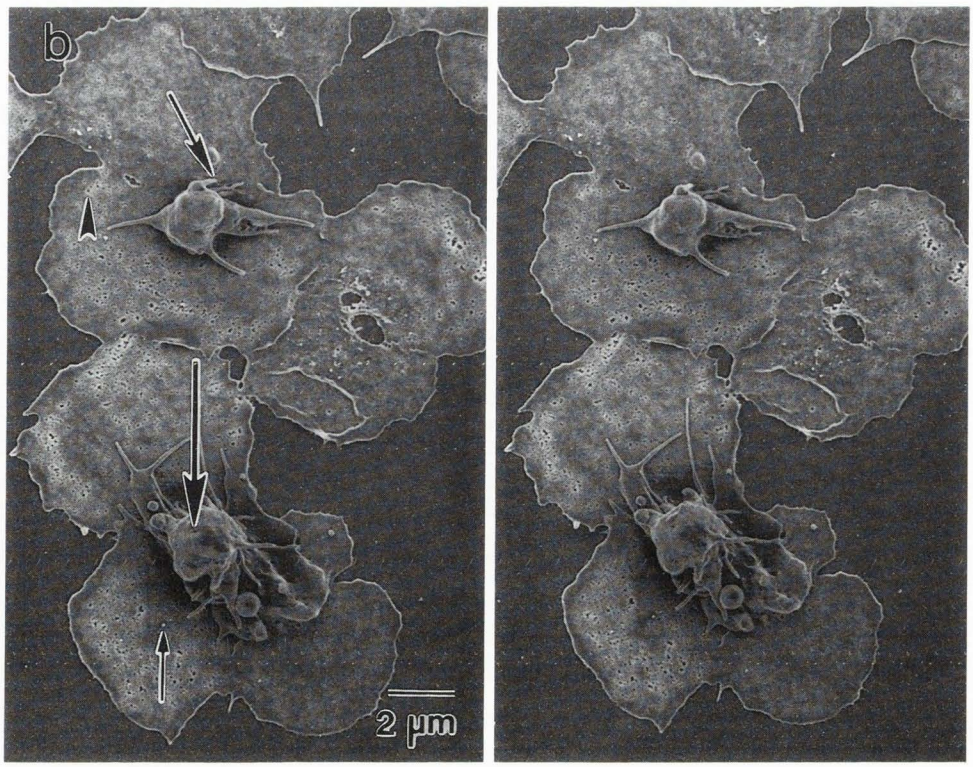

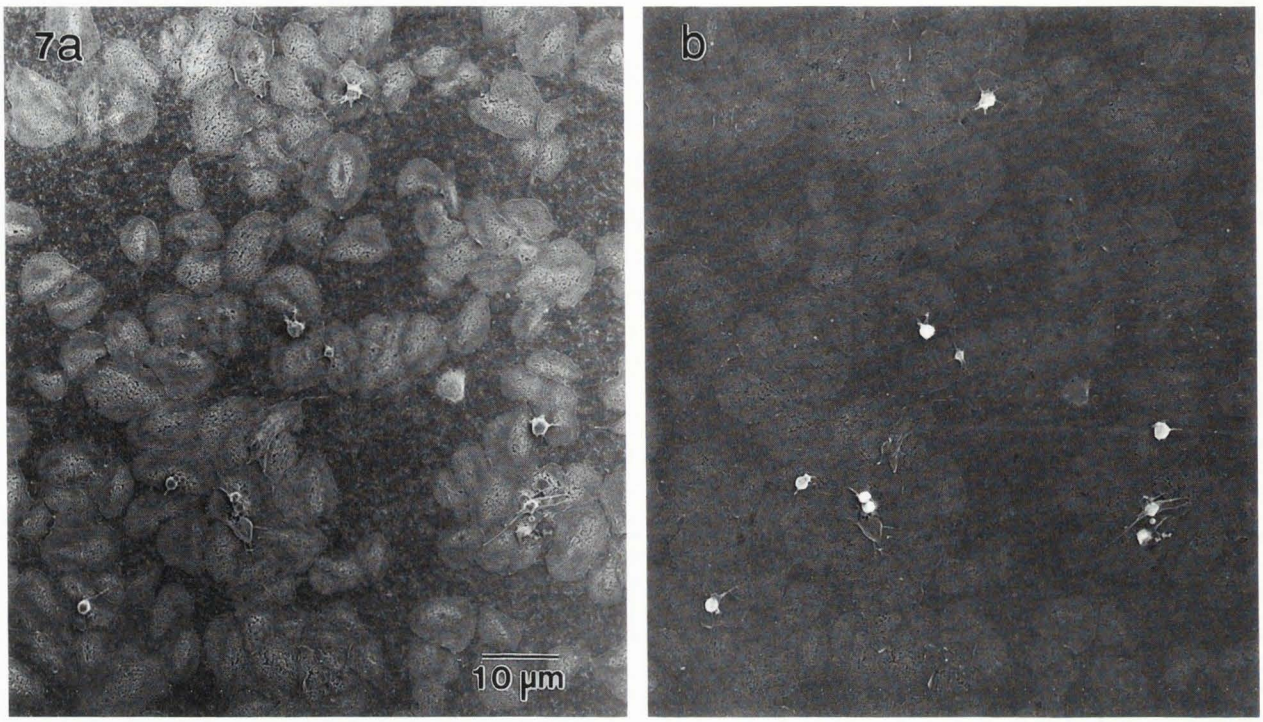
7a
10 µm
b

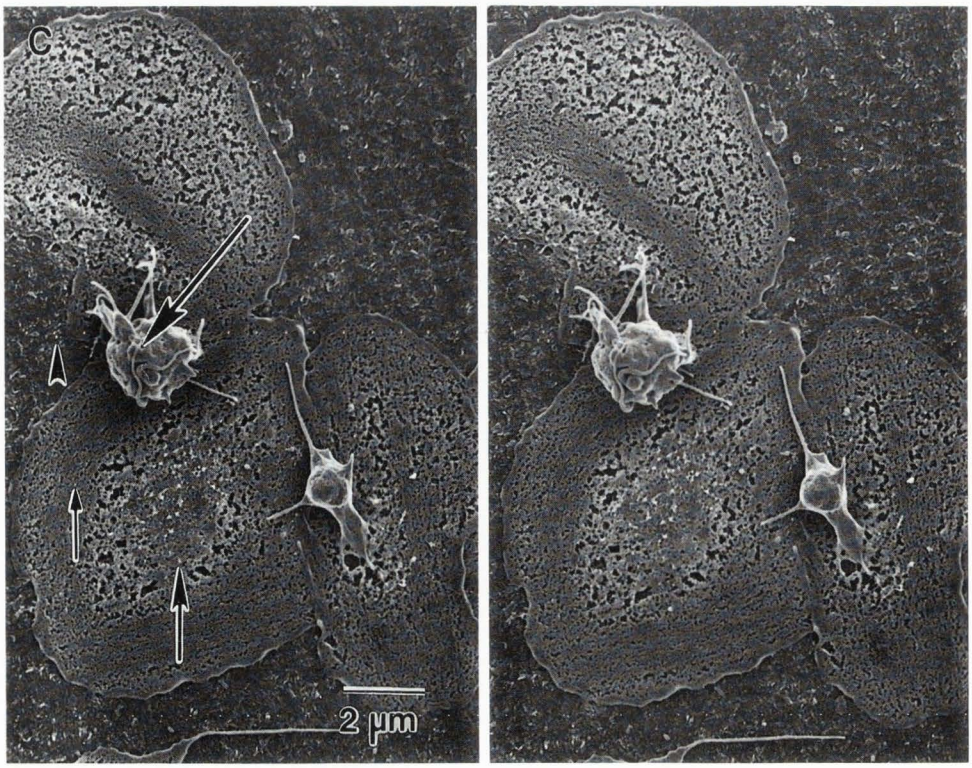
c
2 µm

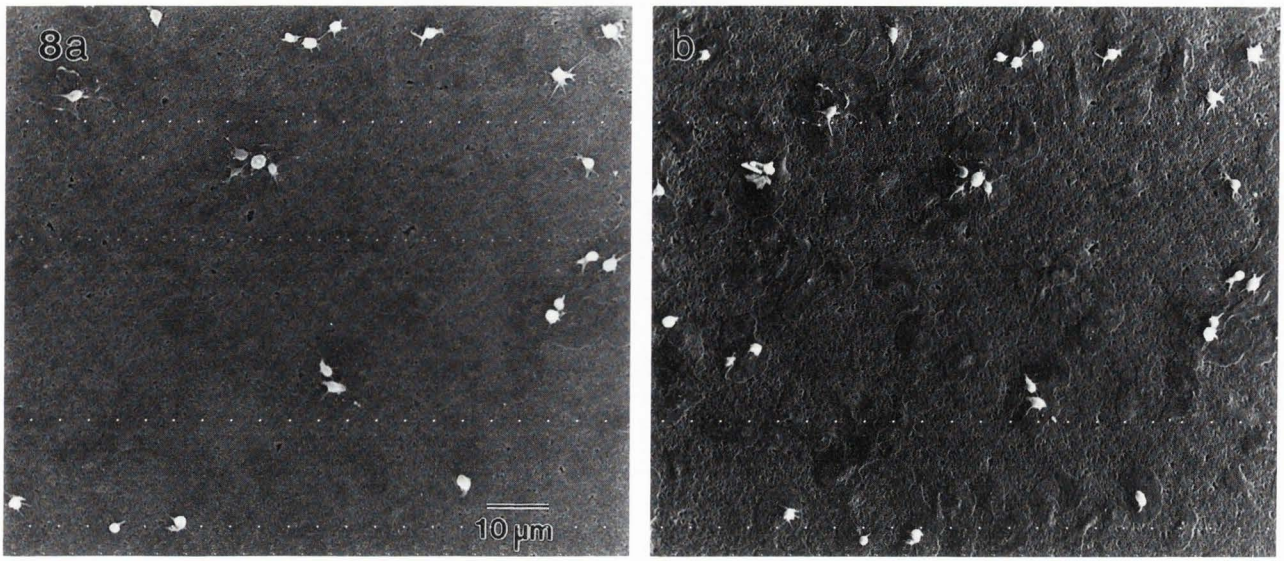

Figure 8 (above). Platelets adherent to CMI-LTIC observed with conventional SEM instrumentation (Hitachi S-570, LaB_6 filament, working distance = 7 mm) at 15 keV and sputter-coated with 10 nm AuPd. (**a**) With no tilt (sample plane perpendicular to the primary electron beam), pseudopodial platelets are easily detected, while fully-spread platelets are nearly invisible. (**b**) The visibility of fully-spread platelets, as well as some surface texture, is significantly improved by tilting the specimen 35° towards the secondary electron detector.

Figure 7 (on the facing page). (**a**) LV-SEM imaging at 1.5 keV shows nearly complete coverage of the CMI-LTIC surface by extremely well spread platelets. Virtually all platelets in contact with the substrate are fully spread, while pseudopodial platelets are adherent to these fully-spread platelets, and generally not in direct substrate contact. (**b**) When imaged at 15 keV, the same fully-spread platelets become much less visible while the thicker pseudopodial platelets greatly increase in brightness and contrast. Ion beam Pt-coated. (**c**) Stereo-pair of central region (imaged at 1.5 keV) shows spread platelets are extremely thin and closely follow the contours of the LTIC substrate. Since the LTIC substrate is not flat, heights are relative to a single reference point on the surface (arrowhead). A point on the outer filamentous zone is 0.20 μm below (small arrow) the reference point, while the highest point at the edge of granulomere of the same platelet is 0.21 μm above (medium arrow), hence the platelet follows the LTIC topography. The highest point on the pseudopodial platelet is 3.9 μm above (large arrow) the reference point. The membranes on the spread platelets appear poorly preserved or disrupted while those of the pseudopodial platelets appear intact and well preserved.

---

of pseudopodial and less spread platelets appeared well preserved.

Discussion

Low-temperature isotropic pyrolytic carbon morphology

LV-SEM examination (Figs. 1a and 1b; 2a and 2b; and 3) reveals a very complex surface topography on LTIC polished and prepared exactly as used in clinical heart valves. Feature sizes' range from 10 nm to 1 μm, with height differences of hundreds of nanometers observed over lateral distances as little as 10 nm. Compared to previously published images obtained with conventional SEM instrumentation [6, 8, 31, 32], the LV-SEM shows a much rougher surface. These different observations can be explained by the physics of image formation as a function of the primary beam accelerating voltage, and other differences between low voltage and conventional (higher voltage) SEM.

As seen in Figure 4, identical regions appear much smoother when imaged with an accelerating voltage of 15 keV, and very similar to previously reported images, as apposed to imaging at 1.5 keV. The primary reason

for the differences between these images is that the emission of the image-forming secondary electrons does not occur at the point where the primary beam scans the surface, due to scattering of the incident electrons in the sample. Briefly, in SEM, the primary electron beam interaction with the sample occurs within a finite pear-shaped volume [30, 38]. Cross-sections of these interaction volumes can be simulated with Monte Carlo calculations of primary electron beam pathways (Fig. 5). Secondary electrons (SE) are generated throughout this volume, and can contribute to image formation if they are close enough to the surface to escape from the solid and be collected by the SE detector. These escape depths vary with atomic number, density, and other parameters, but are typically 10-100 nm in carbon and much less in high density and high atomic number materials. The excitation volume also varies greatly with accelerating voltage, such that the majority of secondary electrons are generated within 10-20 nm of the primary beam impact point at 1.5 keV, while at 15 keV, secondary electrons are generated up to one micrometer away (Fig. 5). This multiple scattering of electrons away from the point of impact of the primary beam creates an image which is a function of the depth of penetration of the primary beam and the escape depth of the SEs. The effect can be quite significant in low density materials such as LTI carbon, and especially on rough samples. For example, 15 keV primary electrons impinging upon a thin vertical feature, such as an LTIC disk (Figs. 1b and 2b), will produce SE emission from the entire disk structure since electrons can escape from the side of the feature. Thus, the resulting image is a complex composite of the material structure averaged over the entire depth of penetration of the primary electron beam. This is sometimes referred to as the "information depth" and can greatly decrease the surface sensitivity of the image. Multiple scattering of the primary beam leading to SE emission away from the incident beam also gives rise to an anomalous increase in the brightness of edges, referred to as "edge effect". At 1.5 keV, both the information depth and edge effects are minimized since the primary beam interaction volume is so much smaller [29, 30, 38].

In conventional SEM, high atomic number coatings such as Au or AuPd, are applied to non-conductive materials to minimize sample charging, and to maximize the production of secondary electrons from surfaces of low atomic number. Since electron paths are much reduced in high atomic number elements, this can significantly decrease information depth and edge effect. For conventional SEM, 10-20 nm or thicker coatings are commonly used, however with LTIC, even a 10 nm coating would obscure considerable fine detail. For example, 10 nm is the distance observed between many disks (Figs. 1b and 2b). It is also unlikely that a uniform coating could be applied to such a rough surface, especially the sides of vertical features, thus some edge effect and depth averaging would still occur.

Since LTIC is somewhat conductive, no metal coatings are required at the low accelerating voltages used with LV-SEM (Fig. 4). However, at 1.5 keV, image resolution appeared to be limited by the spot size of the electron probe at magnifications in excess of about 60,000x. Since spot size in the instrument used rapidly decreases with increased keV, a slightly higher accelerating voltage can substantially improve instrumental resolution [30]. However, this comes at the expense of increased beam penetration into the low atomic number LTIC surface, thereby increasing information depth and edge effect. To partially circumvent this, as well as to provide conductivity for the polystyrene size standards, a 1-2 nm thin coat of Pt was applied. This enabled higher resolution imaging at 2.5 keV with minimal edge effect (Fig. 2b). However, even at a slightly higher accelerating voltage of 3.5 keV, edge effects overshadowed the increased instrumental resolution on these samples (not shown), probably due to uneven coating of this complex topography.

LTIC surfaces have also been examined with STM [14, 36], however the present LV-SEM images show a rougher surface than in these reports. Where we regularly observed height differences of 100-300 nm and more, a recent STM study of biomedical LTIC reported peak-to-valley distances of about 50 nm [14]. However, the similarity of the samples in other studies to those in the present study are unknown. For example, the LTIC used by Feng and Andrade [14] was supplied by a different manufacturer (Sorin Biomedica, Italy) and polished with different protocols than in the present study. Nonetheless, STM and other mechanical tip scanning probe microscopies have a significant disadvantage with rough samples such as LTIC. Although the very tip of an STM or an AFM can be of atomic dimension, the entire scan head is quite large compared to the roughness of LTIC (a typical STM or AFM head is generally pyramidal or cone-shaped and has base and height dimensions on the order of 2-5 μm). Due to this relatively large width, lateral contacts between the scan head and rough surface features prevent the tip from reaching down into narrow spaces. Hence, STM and AFM instrumentation can provide atomic resolution images of mountain tops [14], but are unable to image into narrow valleys or along steep cliffs. Such lateral interactions could artifactually provide the impression that narrow depressions are shallow, when in fact they may be deep. Lateral interactions of scanning tips with sample features can also make features appear much wider than their actual dimensions. This broadening effect has been most extensively described for AFM [33]. Nonetheless,

scanning probe microscopies excel at providing atomic level resolution and nanometer-resolution height measurements, albeit they are limited to samples which are smooth relative to the dimensions of the scanning head, or to scanning the "mountain tops" of rough materials. With SEM, height measurements may be made by measurement of parallax shift from stereo-pair images, however such measurements are generally considered to be less accurate than the lateral resolution [10], as discussed in **Materials and Methods**.

In comparison to previously reported TEM images of LTIC, the present study provides complementary information on material morphology. Although direct comparison is difficult since TEM images are obtained from thin slices through bulk samples, the present images show an organization which is consistent with the previously described isotropic turbostratic structure [32, 41, 49], including the organization and sizes of disks and the crystallite-like aggregates of disks at surfaces (Figs. 1, 2, and 4) and in the bulk (Fig. 3).

Platelet adherence

Platelets attached and spread on CMI and SJM LTIC more than observed on Formvar (Figs. 6a and 6b; and 7a, 7b, and 7c), a material which we regularly use as a positive control for platelet spreading [21, 22]. On both LTIC materials, essentially every platelet in contact with the material was fully spread, and only a few pseudopodial platelets were found adherent to the top of fully-spread material-adherent platelets. In contrast, on Formvar, there was considerable open space which did not have adherent platelets, and there were many less activated pseudopodial platelets on top of Formvar-adherent fully-spread platelets. Since LTIC induces virtually complete spreading of all platelets and near monolayer coverage, in contrast to Formvar, and as the kinetics of platelet substrate-contact are independent of the material, this suggests that the LTIC surface is significantly more sticky for platelet adhesion (and spreading) than are either fully-spread platelets or Formvar.

In order to minimize the number of platelets adherent to platelets and thereby facilitate the imaging of material-adherent platelets, platelet suspensions were rinsed off after 10 minutes incubation. Even so, a few pseudopodial platelets were observed on top of spread platelets adherent to LTIC (and even more on Formvar). In nearly every observation, these secondarily adherent platelets overlay the central regions of individual fully-spread platelets, or overlay the common center of adjacent material-adherent fully-spread platelets in mutual contact (Figs. 6a and 6b). In addition, many pseudopods of these platelets extended away from the substrate for several micrometers (Fig. 6b), thus they would be capable of snagging platelets in suspension and recruiting these into an aggregate. These observations are consistent with light and electron microscopic observations of the mechanism by which spread platelets form a base upon which secondarily adherent platelets aggregate and form a thrombotic center [2, 17]. Hence, LTIC appears to be capable of supporting the platelet-platelet cohesion which is necessary for thrombus growth.

Comparison between platelets adherent to Formvar (Fig. 6a) and LTIC (Fig. 7a) show that the fully-spread platelets on LTIC appear to be spread to a greater extent. Parallax-shift height measurements on stereo-pair micrographs demonstrate that fully-spread platelets on Formvar (Fig. 6b) are 1.0-1.5 μm thick in the vicinity of the granulomere, and about 0.25 μm thick at their thinnest point in more peripheral regions. In contrast, LTIC-adherent platelets are typically only 0.25-0.5 μm at the granulomere region (Fig. 7c), or about half as thick as Formvar-adherent platelets. Stereo imaging also shows that platelets very closely follow the contours of the LTIC substrate. Higher resolution reveals a fragmented holey membrane on fully-spread LTIC adherent platelets (Fig. 7c), while the membranes of pseudopodial platelets in these preparations, and the membranes of all Formvar-adherent platelets including those of fully-spread morphology, appear unfragmented and continuous (Figs. 6b and 7c). Since the membranes of all but LTIC adherent fully-spread platelets appear normal, we believe that the membrane fragmentation is caused by the extreme extent of platelet spreading on LTIC which increases their fragility such that they are unable to survive the rigors of ethanol dehydration and/or drying by the critical point method. We have previously observed similar membrane fragmentation on platelets and other cells when they are exceptionally well spread (unpublished observations).

The excellent clinical history of LTIC suggests that this material must be minimally activating to platelets. This is supported by studies which indicate that few platelets are found adherent to this material, and those which are adherent are in less activated (pseudopodial) morphologies [9, 28]. However, in the present study, we report extensive platelet adhesion and spreading. As the differences in the observed surface roughness between this and previous studies were explained due to the physics of image formation between conventional and LV-SEM, so too may the observed differences in platelet adhesion between this and previous reports. As shown in Figures 7a and 7b, as the accelerating voltage is increased from 1.5 to 15 keV, fully-spread platelets become difficult to detect and essentially "disappear", while the visibility of pseudopodial platelets is enhanced. Since fully-spread platelets on LTIC are less than 0.5 μm thick, and since critical point dried biological tissue

has a density of 0.02-0.3 g/cm^3 [29, 38] which is much lower than LTIC (1.7-2.2 g/cm^3), at 15 keV only a very small fraction of the volume of excitation from the primary electron beam occurs either at the platelet surface or even within its volume. In effect, at 15 keV, the beam goes right through thin fully-spread platelets. The invisibility of the fully-spread platelets is further enhanced since they closely follow the 3-D contours of the LTI carbon. In contrast, the visibility of pseudopodial platelets may be enhanced due to edge effect. Since their thickness is much greater (2-5 μm), the primary beam excitation volume is largely contained within the platelet, where it is capable of producing SEs which can escape throughout the entire platelet surface. Such edge effects with pseudopodial platelets are observed in Figure 7b, where there is little variation in the brightness of entire pseudopodial platelets (the whole platelet appears white), whereas at 1.5 keV, there is minimal edge effect thereby producing images of pseudopodial platelets which vary in their brightness (Fig. 7a).

In previous SEM studies of platelet adhesion to LTIC, it is likely that the samples were coated with 10 nm or more of Au or AuPd prior to SEM examination (this detail of specimen preparation was generally not described), unlike the present samples (Fig. 7). While a metal coating would enhance surface imaging, as discussed above with respect to LTIC surface morphology, a 10-20 nm or greater coating would also obscure surface details especially since fully-spread platelets are very thin and closely follow the LTIC topography. We sought to examine the visibility of LTIC-adherent platelets using such conventional SEM specimen coating and instrumentation. Examination of platelets adherent to LTIC valve leaflets sputter-coated with 10 nm AuPd and imaged at 15 keV (Fig. 8a), as well as at 25 keV (not shown) show that only pseudopodial platelets are readily visible. If SEM instrumental contrast were adjusted to maximize the contrast range of the pseudopodial platelets, as might be done since the low contrast fully-spread platelets are even more difficult to see on the SEM display monitor than on photomicrographs, then the barely visible fully-spread platelets would likely not appear at all in the photomicrographs. However, it is possible to enhance the detection of fully-spread platelets with conventional SEM by tilting the sample at a relatively large angle towards the SE detector. This effect is shown at 0° and 35° of tilt (Fig. 8b). Lesser tilt angles had a minimal effect with the Hitachi 570 instrument used. Similar images were obtained (not shown) with a much older instrument, the JEOL JSM 35C which was first introduced in 1974. The tilting significantly enhances the detection of fully-spread platelets and surface topography by using edge effect as a means to enhance topographic contrast [29, 46].

Summary and Conclusions

In the present study, we report that LTIC polished and prepared for use in valve prosthetics appears much rougher than previously described, with features ranging in size from tens to several hundred nanometers. We also report that platelet adhesion and spreading are very extensive on this material, again in contrast to previous reports. The difference between our observations and previous studies can be explained in terms of the physics of image formation between high-resolution LV-SEM as used in this study, STM, and conventional higher accelerating SEM. Due to the extensive topography of LTIC, the low density and atomic number of platelets and LTIC, the obscuration effects of specimen coating on complex surfaces, and since platelets closely follow LTIC's 3-D contours, with conventional SEM fully-spread platelets provide little contrast and can easily be undetected. As a result, the degree of platelet adhesion and spreading which occurs on LTIC vascular prosthetics may have been previously underestimated, suggesting that platelet interaction with LTIC may play an important role in the thromboembolic properties of these devices. At present, it is unknown whether similarly extensive platelet-LTIC interactions occur *in vivo*, in contrast to this *in vitro* study performed with washed platelets in 1 mg/ml albumin and under zero shear stress conditions. Although the present *in vitro* platelet adhesion model has previously been demonstrated to be predictive of whole blood platelet-material adhesion in *ex vivo* circulation [18, 23], the possibility of thrombus growth occurring on implanted valves must be viewed with caution considering the postulated mechanisms by which albumin adsorption may passivate LTIC surfaces [12, 14, 15] thereby leading to the good clinical efficacy of this prosthetic material.

Acknowledgements

The authors acknowledge Dr. David C. Joy (Univ. Tennessee, Knoxville) for providing computer programs to describe SEM electron-solid interactions, and the Integrated Microscopy Resource in Madison (NIH RR-570) for the use of the LV-SEM. Funding for this work was provided by the National Institutes of Health through HL-37351 to SLG and RMA.

References

[1]. Aebischer P, Goddard MB, Sasken HF, Hunter TJ, Galletti PM (1988) Tissue reaction to fabrics coated with turbostratic carbon: subcutaneous versus vascular implants. Biomaterials **9**: 80-85.

[2]. Albrecht RM, Goodman SL, Simmons SR

(1989) Distribution and movement of membrane-associated platelet glycoproteins: use of colloidal gold with correlative video-enhanced light microscopy, low-voltage high-resolution scanning electron microscopy, and high-voltage transmission electron microscopy. Am J Anat **185**: 149-164.

[3]. Anonymous (1994) 10-plus Years Follow Up of the St. Jude Medical® Mechanical Heart Valve. St. Jude Medical, Inc., One Lillehei Plaza, St. Paul, MN 55117. (4 page compendium report).

[4]. Baier RE, Gott VL, Feruse A (1970) Surface chemical evaluation of thromboresistant materials before and after venous implantation. Trans Am Soc Artif Intern Organs **24**: 19-23.

[5]. Baquey C, Bordenave L, More N, Caix J, Basse-Cathalinat B (1989) Biocompatibility of carbon-carbon materials: blood tolerability. Biomaterials **10**: 435-440.

[6]. Bokros JC (1977) Carbon biomedical devices. Carbon **15**: 355-371.

[7]. Bokros JC, Gott VL, La-Grange LD, Fadall AM, Vos KD, Ramos MD (1969) Correlations between blood compatibility and heparin adsorptivity for an impermeable isotropic pyrolytic carbon. J Biomed Mater Res **3**: 497-528.

[8]. Bokros JC, LaGrange LD, Schoen FJ (1973) Control of structure of carbon for use in bioengineering. In: Chemistry and Physics of Carbon. Walker PL, Jr., Thrower PA (eds.). Marcel Dekker, New York. pp. 103-171.

[9]. Borovetz HS, Griffith BP, Phillips L, Jr., Haubold AD, Hercules DM, Hung TK, Hardesty RL (1978) Scanning electron microscopic and surface analytical study of an isotropic vapor deposited carbon film on microporous membranes. Scanning Electron Microsc **1978**;II: 85-94.

[10]. Boyde A (1974) Three-dimensional aspects of SEM images. In: Scanning Electron Microscopy. Wells OC (ed.). McGraw-Hill, New York. pp. 277-307.

[11]. Chignièr E, Monties JR, Butazzoni B, Dureau G, Eloy R (1987) Haemocompatibility and biological course of carbonaceous composites for cardiovascular devices. Biomaterials **8**: 18-23.

[12]. Chinn JA, Phillips RE Jr., Lew KR, Horbett TA (1994) Fibrinogen and albumin adsorption to Pyrolite® carbon. Trans Soc Biomat **17**: 250 (abstract).

[13]. Edmunds L, Jr. (1987) Thrombotic and bleeding complications of prosthetic heart valves. Ann Thorac Surg **44**: 430-445.

[14]. Feng L, Andrade JD (1993) Surface atomic and domain structures of biomedical carbons observed by scanning tunneling microscopy (STM). J Biomed Mater Res **27**: 177-182.

[15]. Feng L, Andrade JD (1994) Protein adsorption on low temperature isotropic carbon. Biomaterials **15**: 323-333.

[16]. Fernandez J, Laub GW, Adkins MS, Anderson WA, Chen C, Bailey BM, Nealon LM, McGrath LB (1994) Early and late-phase events after valve replacement with the St. Jude Medical prosthesis in 1200 patients. J Thorac Cardiovasc Surg **107**: 394-406.

[17]. Goodman SL, Albrecht RM (1987) Correlative light and electron microscopy of platelet adhesion and fibrinogen receptor expression using colloidal-gold labeling. Scanning Microsc **1**: 727-734.

[18]. Goodman SL, Cooper SL, Albrecht RM (1985) Surface activation of platelets from humans, canines, and macaques. In: Progress in Artificial Organs. Nose Y, Kjellstrand C, Ivanovich P (eds.). International Society Artificial Organs Press, Cleveland. pp. 1050-1055.

[19]. Goodman SL, Cooper SL, Albrecht RM (1989) Polyurethane support films: structure and cellular adhesion. Scanning Microsc Suppl **3**: 285-294.

[20]. Goodman SL, Cooper SL, Albrecht RM (1991) The effects of substrate-adsorbed albumin on platelet spreading. J Biomater Sci Polym Ed **2**: 147-159.

[21]. Goodman SL, Cooper SL, Albrecht RM (1993) Integrin receptors and platelet adhesion to synthetic surfaces. J Biomed Mater Res **27**: 683-695.

[22]. Goodman SL, Grasel TG, Cooper SL, Albrecht RM (1989) Platelet shape change and cytoskeletal reorganization on polyurethaneureas. J Biomed Mater Res **23**: 105-123.

[23]. Goodman SL, Lelah MD, Lambrecht LK, Cooper SL, Albrecht RM (1984) *In vitro* vs. *ex vivo* platelet deposition on polymer surfaces. Scanning Electron Microsc **1984**;I: 279-290.

[24]. Goodman SL, Li C, Pawley JB, Cooper SL, Albrecht RM (1988) Surface and bulk analysis of phase-segregation in polyurethanes by electron microscopies. In: The Surface Characterization of Biomaterials. Ratner BD (ed.). Elsevier, Amsterdam. pp. 281-295.

[25]. Goodman SL, Park K, Albrecht RM (1990) A correlative approach to colloidal gold labeling with video-enhanced light microscopy, low voltage scanning electron microscopy and high voltage electron microscopy. In: Colloidal Gold: Methods and Applications. Hayat MA (ed.). Academic Press, San Diego. pp. 369-409.

[26]. Gott VL, Whiffen JD, Dutton RC, Koepke DE, Daggett RL, Young WP (1964) The anticlot properties of graphite coatings on artificial heart valves. Carbon **1**: 378-382.

[27]. Haubold AD (1983) Blood/carbon interactions. Am Soc Artif Intern Organs (ASAIO) J **6**: 88-92.

[28]. Haubold AD, Shim HS, Bokros JC (1981) Carbon in medical devices. In: Biocompatibility of Clinical Implant Materials **2**. Williams DF (ed.). CRC Press,

Boca Raton. pp. 3-42.

[29]. Joy DC (1984) Beam interactions, contrast and resolution in the SEM. J Microsc **136**: 241-258.

[30]. Joy DC, Pawley JB (1992) High-resolution scanning electron microscopy. Ultramicroscopy **47**: 80-100.

[31]. Kaae JL (1975) Microstructures of isotropic pyrolytic carbon. Carbon **13**: 55-62.

[32]. Kaae JL (1985) The mechanism of the deposition of pyrolytic carbon. Carbon **23**: 665-673.

[33]. Lal R, John SA (1994) Biological applications of atomic force microscopy. Am J Physiol **266**: C1-C21.

[34]. Loftus JC, Choate J, Albrecht RM (1984) Platelet activation and cytoskeletal reorganization: high voltage electron microscopic examination of intact and Triton-extracted whole mounts. J Cell Biol **98**: 2019-2025.

[35]. Marchon B, Ferrer S, Kaufman DS, Salmeron M, Siekhaus W (1987) The surface topography of pyrolytic carbons and of gold thin films by scanning tunneling microscopy: Grain boundaries and surface defects. Thin Solid Films **154**: 65-73.

[36]. Marchon B, Salmeron M, Siekhaus W (1989) Observation of graphitic and amorphous structures on the surface of hard carbon films by scanning tunneling microscopy. Physical Rev B **39**: 12907-12910.

[37]. Nagatani S, Saito S (1986) Instrumentation for ultra high-resolution scanning electron microscopy. In: XI Intl Cong Elec Micro. Imura T, Maruse S, Suzuki T (eds.). Jap Soc Elec Micro, Kyoto. pp. 2101-2104.

[38]. Pawley JB (1992) LVSEM for high-resolution topographic and density contrast imaging. In: Advances in Electronics and Electron Physics. Hawkes P (ed.). Academic Press. pp. 203-273.

[39]. Pawley JB, Erlandsen SL (1989) The case for low voltage high-resolution scanning electron microscopy of biological samples. Scanning Microsc Suppl **3**: 163-178.

[40]. Pawley JB, Walther P, Shih SJ, Malecki M (1991) Early results using high-resolution, low-voltage, low-temperature SEM. J Microsc **161**: 327-335.

[41]. Pollmann E, Pelissier J, Yust CS, Kaae JL (1977) Transmission electron microscopy of pyrolytic carbon. Nuclear Technol **35**: 301-309.

[42]. Salzman EW, Lindon J, Brier D, Merrill EW (1977) Surface-induced platelet adhesion, aggregation, and release. In: The Behavior of Blood and its Components at Interfaces. Vroman L, Leonard EF (eds.). Annals of the New York Academy of Sciences, New York. Volume **283**, pp. 114-127.

[43]. Schoen FJ (1983) Carbons in heart valve prostheses: foundations and clinical performance. In: Biocompatible Polymers, Metals, and Composites. Szycher M (ed.). Technomic, Lancaster, PA. pp. 239-261.

[44]. Smith KL, Black KM (1984) Characterization of the treated surfaces of silicon alloyed pyrolytic carbon and silicon carbide. J Vac Sci Technol **A2**: 744-747.

[45]. Tangen O, Berman HJ, Marfey P (1971) Gel filtration. A new technique for separation of blood platelets from plasma. Thromb Diath Haemorrh **25**: 268-278.

[46]. Wells OC (1974) Scanning Electron Microscopy McGraw-Hill, New York. pp. 62-64.

[47]. Whalen RL, Jeffery DL, Norman JC (1973) A new method of *in vivo* screening of thromboresistant biomaterials utilizing flow measurement. Trans Am Soc Artif Intern Organs **19**: 19-23.

[48]. Willison JHM, Rowe AJ (1980) General considerations in the replication of specimens. In: Replicas, Shadowing and Freeze-Etching Techniques. Willison JHM, Rowe AJ (eds.). North-Holland, Amsterdam. pp. 95-105.

[49]. Yust CS, Krautwasser HP (1975) Transmission electron microscopy of propene-derived pyrolytic carbon coatings. Carbon **13**: 125-133.

Discussion With Reviewers

G.L. Picciolo: Have you done any tests with unpolished LTIC samples? Are the observed disks and disk clusters related to the polishing process? Is the adhesion of the platelets related to it?

F.J. Schoen: In **Results**, the structural units of LTIC are described as discoid. In previous studies by SEM of the detailed structure of LTIC, the unit of structure was shown to be a sphere. Are these observations in disagreement?

Authors: The LTIC materials were polished exactly as per the manufacture of prosthetic valves. Since we have not examined any unpolished samples, it is difficult to comment on how polishing influences morphology. Nonetheless, 3-D examination reveals spherical structures in the lower sample regions (such as to the left of the scale marker in Fig. 1b) while disks and disk clusters are generally found in the upper regions of the sample. This suggests that polishing may have a role in the appearance of the disks, perhaps exposing them to view. It is difficult to ascertain if our observations of disks, in contrast to spheres, are in disagreement with earlier reports since apparent differences could be due to other factors, including dissimilar LTIC materials and polishing protocols, differences in imaging physics at low and high voltage SEM, differences in resolution, shape smoothing due to conductive coatings, and perhaps that unless viewed end on or as a stereo-pair it can be impossible to discriminate between a disk and a sphere. We have also not examined platelet interaction with unpolished samples.

F.J. Schoen: These studies described herein should clearly be extended to material that has previously been implanted *in vivo*, either experimentally or clinically. How should explants be prepared to optimize information content?

Authors: We completely agree that explants should be examined and are quite interested in doing so. The major issue in optimizing information content is to ensure that surface imaging is not compromised. Hence, the protocol described in this paper is appropriate, especially with respect to limiting the thickness of any conductive coating and imaging at low accelerating voltages such as the 1.5-2.5 keV used herein. Since protein adsorption, platelet adhesion, and fibrin clotting can occur rapidly post mortem, it is absolutely necessary to ensure that such explanted samples are free of artifactual thrombus formation. Hence, the first step might be to perfuse with anticoagulants (as appropriate with experimental implants), followed by explantation and rinsing in an appropriate isosmotic buffer to prevent non-specific protein adsorption and cell adhesion. This is then followed by fixation. While immediate fixation in EM grade glutaraldehyde followed by careful dehydration and critical point drying are certainly desirable, this may be difficult with clinical explants since such fixatives and instrumentation may not be readily available. In this case, it would be necessary to prevent the explant from drying by keeping it in the buffer if fixative is not immediately available, and refrigerate (do not freeze since this would cause ice crystal damage). Otherwise, fix in buffered glutaraldehyde, formaldehyde or formalin (listed in decreasing suitability) until complete fixation in electron microscopy grade reagents is possible.

F.J. Schoen: Despite the extensive platelet spreading observed in the present studies, the clinical thromboresistance of LTIC is excellent relative to that of other materials. Does this detract from the utility of *in vitro* platelet adhesion studies, since their predictability in this case is low?

H.S. Borovetz: The authors state that the *in vitro* platelet adhesion model used in this work has previously been shown to be predictive of whole blood platelet-material adhesion *in vitro*. Yet one would have expected a different finding than Figure 7 for LTIC especially when compared to the positive control. To what do the authors attribute this apparent discrepancy and why does their *in vitro* model appear not to be predictive for LTIC? Perhaps the issue of biocompatibility of LTIC (and versus Formvar) should be viewed not simply from the point of view of the single layer of attached platelets, but also from the point of view of aggregation. To investigate these phenomena the authors would need to characterize the platelet receptors IIb-IIIa and Ib in their studies, which is presumably beyond the scope of this work.

Authors: The clinical relevance of the present study is that LTIC is not necessarily passive with respect to platelet adhesion, thus platelet interaction with this material should be reexamined to understand its good clinical thromboresistance. With respect to the *in vitro* platelet model, it is unknown how predictive it is in the present case since explants have not been examined, as addressed in the previous question by Dr. Schoen. For example, it is not known if spread platelet monolayers form on LTIC *in vivo*, although others have shown similarly significant platelet interaction and spreading on LTIC *in vitro* [42]. We agree completely with Dr. Borovetz's comment that one must consider platelet aggregation, and in particular the activity of the adhesion and aggregation receptors glycoprotein (GP) Ib and GP IIb-IIIa. We have previously examined GP IIb-IIIa for a potential role in controlling the extent of platelet surface aggregation on biomaterials [2, 17], although we have yet to do so for LTIC.

H.S. Borovetz: LTIC is a very successful clinical biomaterial, however the platelet data would seem to be in contradiction to this clinical finding (Figs. 6a and 6b; and 7a, 7b, and 7c). These pictures suggest that there is essentially total coverage of the LTIC surface by platelets, and in fact much greater coverage is noted for LTIC than occurs on the Formvar surface (which is used as a positive control). Have the authors quantified the numbers of platelets which attach to the LTIC surface? The authors are aware that Cooper and coworkers have provided such data for other biomaterials using a radiolabeled platelet protocol [Lelah MD, Lambrecht LK, Cooper SL (1984) A canine *ex vivo* series shunt for evaluating thrombus deposition on polymer surfaces. J Biomed Mater Res 18: 475-496; Cooper SL, Fabrizuis DJ, Grasel TG (1987) Methods of assessment of thrombus *ex vivo*. In: Blood in Contact with Natural and Artificial Surfaces. Leonard EF, Turitto VT, Vroman L (eds.). Annals New York Acad Sci **516**: 572-585]. Can a comparison be made between that data and the present LV-SEM analyses?

Authors: A more complete analysis of platelet interactions with LTIC and the clinical ramifications of this work has been submitted for publication. In this work, we report higher numbers and considerably greater platelet spread areas on LTIC materials than on Formvar. However, it is not possible to directly compare these results to *ex vivo* findings. In our earlier studies, comparing *in vitro* and *ex vivo* platelet adhesion on polymers, we found that while platelet morphology *in vitro* was predictive of *ex vivo* morphology, there was no predictability for the extent of platelet deposition (the num-

bers of adherent platelets). This was previously explained as being due to the great differences in platelet-surface transport occurring in a static (non-flowing) *in vitro* model as compared to transport in *ex vivo* circulation [23].

G.L. Picciolo: The use of human donor albumin or at least pooled human albumin versus commercially available human albumin could be used. This may or may not show differences with the adsorption of platelets to the albumin-treated LTIC as with its use in platelet suspension and extraction steps of the procedure. Bovine always seems like a problem for the cross-species interactions, although I realize most research laboratories still use it, particularly due to the possibilities of infectious disease transmission with human products. Is there any literature on this point which does not depend on the use of the sensitive methods of adhesion detection you have described? This may or may not be worth an additional experiment at a later time.

Authors: These are important issues, especially considering the proposed mechanism in which albumin adsorption passivates LTIC to platelet adhesion *in vivo* [12, 14, 27]. Experiments to examine this are in progress. With respect to the differences between human and bovine albumin on platelet adhesion and spreading, we have previously reported that there are some small differences in platelet spreading on polymers in the presence of bovine versus human albumin [20]. However, the major result of that study was that the polymeric biomaterial, and not the adsorbed albumin, has the primary role in determining the platelet response.

K. Murata: You try to explain differences between the SE image contrasts at low and high energies from the localization of electron penetration. But, this does not make the differences clear. In more details, you may need to discuss the differences based on the electron incidence angle dependence of the secondary emission intensity at low and high energies. Have you studied this dependence?

Authors: At high accelerating voltages, the incident beam produces SE emission from a much larger volume than at low accelerating voltages (Fig. 5). The resulting emitted SEs come from both some distance below the sample surface, and from some lateral distance from the probe. This produces an image which is "averaged" over a region comparable in size to the excitation volume, which at high keV is larger than many of the structural features of the material. Thus, at higher accelerating voltages both lateral and depth sensitivity are significantly decreased. When the incident beam is perpendicular to the sample, the depth to which SE excitation occurs is maximal as compared to when the incident beam is oblique to the surface [29, 30, 38]. Surface sensitivity may thus be increased by altering the angle of incidence, as shown in Figure 8 for conventional SEM, in which the incidence angle was decreased by tilting the sample. In the present study, it was not necessary to use sample tilt with LV-SEM to provide adequate contrast.